Erythrocyte-shape evolution recorded with fast-measurement NMR diffusion-diffraction

Guilhem Pages, David Szekely, Philip W. Kuchel

Original Research

Erythrocyte-Shape Evolution Recorded with Fast-Measurement NMR Diffusion–Diffraction

Guilhem Pages, PhD, David Szekely, BS, and Philip W. Kuchel, PhD*

Purpose: To monitor red blood cell (RBC) shape evolution by ^1H_2O diffusion–diffraction NMR in time steps comparable to those required for the acquisition of a ^{31}P NMR spectrum; thus, to correlate RBC mean diameter with ATP concentration after poisoning with NaF.

Materials and Methods: Pulsed-field gradient-stimulated echo (PFGSTE) diffusion experiments were recorded on ^1H_2O in RBC suspensions. Under conditions of restricted diffusion, *q*-space experiments report on mean RBC diameter. To decrease experiment time, the phase cycling of radiofrequency (RF) pulses was cut to two transients by using unbalanced pairs of gradient pulses. Data processing used a recent digital filter. Differential interference contrast (DIC) light microscopy also recorded shape changes. ^{31}P NMR spectroscopy gave estimates of mean ATP concentration.

Results: NaF caused RBC-shape evolution from discocytes, through various forms of echinocytes, to spherocytes, over ~6 h and ~10 h at 37°C and 25°C, respectively. ATP declined to ~0.5 its normal concentration before the first stage of discocyte transformation; the concentration was 0.0 after ~1.5 h and 3.0 h, respectively, at the two temperatures.

Conclusion: RBC shape was readily monitored by NMR with a temporal resolution that was useful for correlations with both DIC microscopy and ^{31}P NMR spectra.

Key Words: *q*-space imaging; pulsed-field gradient-stimulated echo NMR; red blood cell shape; apoptosis
J. Magn. Reson. Imaging 2008;28:1409–1416.

THERE IS CONSIDERABLE CURRENT INTEREST in the relationship between the shape of a cell and its underlying metabolic state (1). The internally programmed and regulated transformation of cell shape in apoptosis is well known, but a means of quantifying the average-cell geometry in milliliter-size samples with time has been elusive. A phenomenon that is biochemically related to apoptosis, that occurs in the absence of the usual nuclear and mitochondrial influences (because this cell does not have these organelles), is the sequential shape transformation that occurs in the human erythrocyte (red blood cell; RBC) under experimentally well-defined conditions (2,3).

Normal human RBCs have a characteristic biconcave disc shape, like a flattened cylinder that is depressed in the center with a dumbbell-shaped cross section. The normal cell can evolve either to a spherocyte (spheres) via different echinocytic forms (spherical shapes with rounded then spiky protrusions) or to stomatocytes of swollen cup-shaped cells. Bessis (4) classified these different cells according to their shape and number of protrusions. Shape change in RBCs can be either imposed from outside by hydrodynamic and related effects in the vascular system, or on a longer time scale (minutes) in response to metabolic changes and the chemical environment (5,6); for example, addition of sodium fluoride to RBCs inhibits enolase in the glycolytic pathway, thus decreasing the supply of ATP (7). This decline appears to be related to the change in shape from a discocyte, to various forms of echinocyte, and finally to a spherocyte.

Pulsed-field gradient-stimulated echo (PFGSTE) NMR experiments are able to estimate RBC dimensions and intercellular separation from the "diffusion–diffraction" pattern of water (8). This is achieved from the data representing the NMR signal decay vs. the "spatial wave-number vector" $\mathbf{q} = (2\pi)^{-1}\,\gamma\,\delta\,\mathbf{g}$, where γ is the magnetogyric ratio of the nuclei, δ is the duration of the magnetic field gradient pulses used in the experiment, and $\mathbf{g}$ is the magnetic field gradient vector of magnitude g. Such a "*q*-space plot" (9) displays a minimum, then a maximum, and then subsequent minima and maxima (10–12). A direct mathematical relationship exists between the position of these minima and the average mean diameter of the cells. It has already been shown that the PFGSTE NMR experiment is able to probe RBC shape (12) and, especially, to distinguish discocytes and spherocytes from their respective characteristic *q*-space plots; to characterize CNS structure (13–16) and to study their pathologies (17–19).

Additional Supporting Information may be found in the online version of this article.

School of Molecular and Microbial Biosciences, University of Sydney, Sydney 2006 NSW, Australia.

Contract grant sponsor: Discovery Grant from the Australian Research Council.

*Address reprint requests to: P.W.K., School of Molecular and Microbial Biosciences, University of Sydney, Sydney 2006 NSW, Australia. E-mail: p.kuchel@mmb.usyd.edu.au

Received May 13, 2008; Accepted August 13, 2008
DOI 10.1002/jmri.21588
Published online in Wiley InterScience (www.interscience.wiley.com).

From a *q*-space plot, it is also possible to estimate the average propagator (20) (the probability distribution of displacement) by applying a Fourier transform to the data (21). The postprocessing applied to the data (21) consists of applying a Blackman Harris window function to the PFGSTE data, thus enhancing the relative weight of coherence features in the center of the plot. Then, the second derivative of this modified signal is taken prior to Fourier transformation; the latter procedure is a high-pass filter because the output function becomes multiplied by the dependent variable raised to the second power. The automation of data processing avoids manual measurements and subjective bias in identifying critical values (minima, maxima and plateaux) in the *q*-space plots.

One of the major drawbacks of the PFGSTE NMR *q*-space experiment is its overall execution time. Due to the requirement to phase cycle the radiofrequency (RF) pulses it is necessary to record at least 16 transients per magnetic field gradient value. Therefore, the acquisition time for a typical *q*-space data set has been ~1 h (12). A few methods have been developed to decrease the experiment time (22) to record a diffusion experiment under "fast" conditions. In this context, we adapted the pulse sequence described by Pelta et al. (23) to the special conditions dictated by RBC suspensions with extreme restriction of ^1H_2O diffusion. The pulse sequence is a bipolar PFGSTE one (24), with each pair of gradient pulses unbalanced by a relative intensity factor, α. This strategy suppresses unwanted magnetization–coherence pathways, and allows a spectrum to be based on only one transient per gradient strength, saving time by a factor of 16.

Our aim was to implement and evaluate a diffusion-measurement method to record *q*-space data over the minute time scale to probe mean RBC diameter at a rate comparable to that achievable with ^{31}P NMR spectra that report on metabolism. We also quantified the kinetics of RBC shape evolution with differential interference contrast (DIC) light microscopy and related them, and the *q*-space data, to the metabolic state of the cells.

MATERIALS AND METHODS

RBC Preparation

Human RBCs were obtained by venipuncture from the cubital-fossa of a healthy donor (G.P.). The cells were centrifugally washed three times (10 min, 3000 × *g*, 5°C) in a solution of isotonic saline consisting of 154 mM NaCl, 10 mM glucose, 283 mOsmol kg^{-1}, or with 154 mM NaF replacing the NaCl, to observe discocytes or spherocytes, respectively. The buffy coat was removed by vacuum pump aspiration. To transform the hemoglobin into a stable low-spin diamagnetic state, the cells were bubbled with CO for 15 min prior to the final washing step. For discocytes, this final wash was performed after the addition of 0.5% w/v of bovine serum albumin (BSA) (pH 7.4) to the isotonic saline solution. In all cases the packing density (hematocrit) of RBCs was adjusted to 0.70. For the experiments involving NaF the final concentration inside the sample was 20 mM.

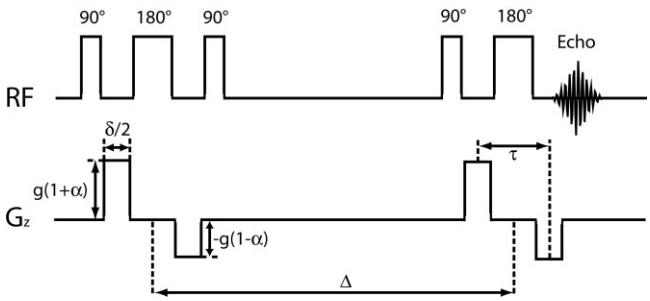

Figure 1. Fast measurement of diffusion, pulse sequence as described by Pelta et al. (23). Notation: RF denotes the radiofrequency time train; G_z the magnetic field gradient pulse time train; δ is the gradient-pulse duration; *g* is the gradient amplitude; Δ is the diffusion time (time between the midpoints of the two diffusion-encoding periods); τ is the time between the midpoints of the antiphase field gradients within a given diffusion-encoding period; and α is the "unbalancing" factor of the gradient pulses that obviates the use of EXORCYCLE phase cycling.

Diffusion–Diffraction NMR Experiments

The RBCs were added to an 8-mm external diameter flat-bottomed glass NMR tube (Wilmad, Buena, NJ, USA). A Teflon vortex plug was inserted into the tube and positioned to give a sample height of 1 cm, corresponding to the length over which the field gradients were linear. The flat-bottomed tube was inserted into a 10-mm outer diameter NMR tube (Wilmad). Carbon tetrachloride was added inside the 10-mm NMR tube; this has a magnetic susceptibility close to those of the RBC suspension and glass, thus avoiding large magnetic susceptibility discontinuities that give rise to magnetic field inhomogeneities at the boundaries in the sample.

The NMR experiments were carried out on a Bruker (Karlsruhe, Germany) DRX 400 NMR spectrometer operating at 400.13 MHz for ^1H detection. The magnet was from Oxford Instruments (Oxford, UK), wide-bore 9.4 T; the spectrometer was equipped for diffusion measurements with a Bruker power supply and probe that delivered magnetic field gradient pulses up to 9.8 T m^{-1} in the direction of $\mathbf{B}_0$. The probe temperature was set to 25°C or 37°C, and the duration of an RF $\pi/2$ pulse was ~22 μsec.

PFGSTE and fast (23) NMR diffusion experiments were recorded with 16 and 2 transients, respectively, per gradient strength. In all cases, 64 steps of field gradient were used and the diffusion time Δ was 20 msec. To obtain the same maximum *q* value for both experiments, δ was set to 2.0 msec and 3.0 msec, and the maximum gradient strength was set to 8.4 T m^{-1} and 8.1 T m^{-1} for PFGSTE and fast NMR diffusion experiments, respectively, with a constant α factor fixed to 0.3. The signal-to-noise ratio was greater than 600:1 for the first spectrum in the *q*-space series, at both temperatures. The fast NMR diffusion pulse sequence is given in Figure 1.

The NMR data consisted of 2K complex points over a spectral width of 4.1 kHz. A 5-Hz exponential line-broadening factor was applied to the data prior to Fourier transformation, and no zero filling was used. *q*-Space plots were processed according to Kuchel et al. (21) using a program written in *Mathematica*.

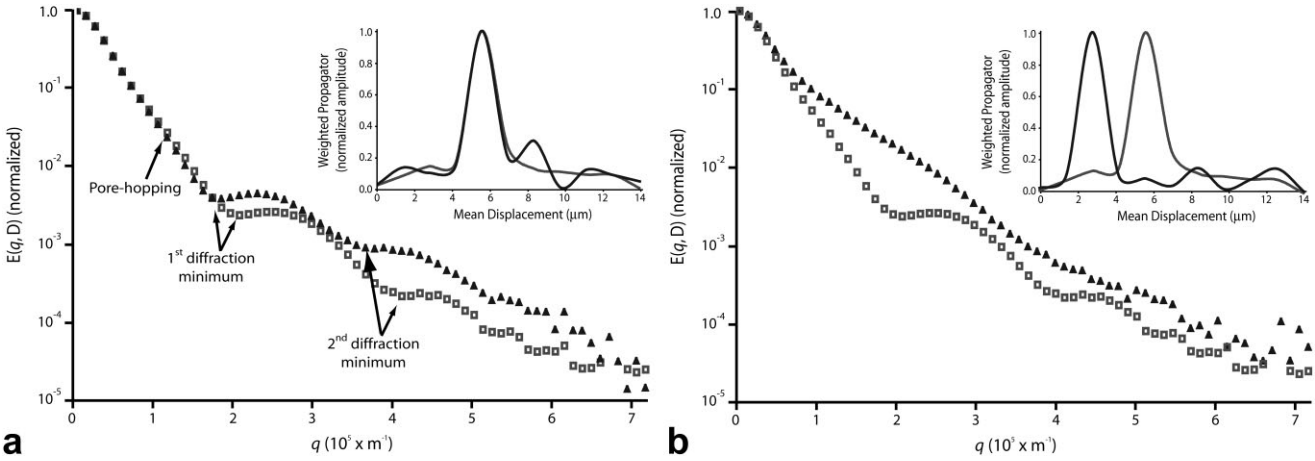

Figure 2. Characteristic *q*-space plots from RBC samples. (**a**) Comparison of both classical (▲) and fast-diffusion (□) PFGSTE pulse sequences, and (**b**) influence of RBC shape as recorded by fast-diffusion pulse sequence that were predominantly discocytes (□) and spherocytes (▲). The insets show the displacement distributions for both graphs after applying the processing described by Kuchel et al. (21). The gray line is the weighted distribution for discocytes recorded by fast-measurement PFGSTE in (**a**) and (**b**), whereas the black line corresponds to (**a**) classical PFGSTE experiment and (**b**) spherocyte shape cells. Curves were scaled to give 1.0 for the amplitude of the highest peak.

^{31}P NMR Experiments

A 10-mm broadband probe, with the inner coil tuned to the frequency of ^{31}P, and the outer coil to the frequency of ^{1}H, was used. Triethyl phosphate (TEP) of a known concentration was added to all samples as a ^{31}P chemical-shift (0.44 ppm) and intensity reference (4 mM) (25). Spectra were acquired with rapid RF pulsing and continuous broadband proton decoupling (WALTZ-16) (26). The acquisition time was 0.34 sec and the spectral width was fixed at 6000 Hz; the relaxation delay was 1 sec. The number of transients per spectrum was 630 to have an experiment time of 15 min; the signal-to-noise ratio of the ATP-γP peak at the beginning of the experiments was 10 and 14, at 25°C and 37°C, respectively. The variable temperature unit was set to 23°C and 35°C to give sample temperatures of 25°C and 37°C, respectively, due to the heating associated with broadband decoupling. Free induction decays were zero-filled with 8192 data points and 6 Hz exponential multiplication was applied before Fourier transforming the data.

Microscope Experiments

Circular glass coverslips (42 × 0.17 mm) were treated with 2 mM poly-L-lysine (Sigma, St. Louis, MO, USA) the excess of which was subsequently washed off; the coverslips were then dried and treated with 0.5% w/v BSA saline. Aliquots of 40 μL RBCs suspended in 0.5% w/v BSA saline, or treated with NaF (20 mM) (hematocrit ~0.005) were transferred into an 8-mm diameter well in a 0.3-mm thickness copper spacer, coated with high-vacuum grease, and sandwiched between two coverslips. The sample in the excess volume sealed the chamber. The cover slips were fixed into a PeCon perfusion chamber and temperature controlled using a PeCon Tempcontrol 37-2 digital unit. The DIC images (Fig. 3) were recorded digitally at 25°C and 37°C with a 100× oil immersion objective on a Zeiss Axiovert 200M microscope with a monochrome HSm digital camera (Zeiss, Jena, Germany). The images and movies were exported using *Stallion* (3i; Intelligent Imaging Innovations Inc, Denver, CO, USA) software and the classification of the RBCs types was done "by eye."

RESULTS

Fast Diffusion-Measurement NMR Setup

Fast diffusion-measurement pulse sequences have been developed to estimate the diffusion coefficient of solutes and solvents in liquids. In their work, Pelta et al. (23) used a diffusion probe that delivered *z*-gradients of strengths up to 0.3 T m^{-1}. Our first challenge was to implement this pulse sequence to use gradients 30 times higher, because signal attenuation is much less when water is restricted in its motion in RBC suspensions. The unbalanced pulse pairs are used to suppress unwanted signals in the x′,y′-plane. However, if the absolute difference between the two last gradient pulses is insufficient, residual signal survives, increasing the apparent amplitude. To obviate this problem, we used a high value of α, equal to 0.3. Running experiments with only one transient per gradient strength did not give useable results; the *q*-space plots varied randomly and the diffraction minima were not evident. Therefore, we doubled the number of transients per gradient strength and cycled the phase of the third 90° RF pulse by 180°. This gave clearly delineated diffraction minima in *q*-space plots (Fig. 2). The second transient, phased by 180°, brought about removal of residual unwanted signals that could have been due to imperfect RF pulse-length calibration. The diffusion–diffraction pattern obtained by using the fast-measurement pulse sequence was compared with one obtained by using a classical PFGSTE pulse sequence (Fig. 2a). Both experiments showed two clear diffraction minima that would be characteristic of restricted diffusion of water inside RBCs. However, there was a slight difference in the position of the minima in each case. From conventional PFGSTE

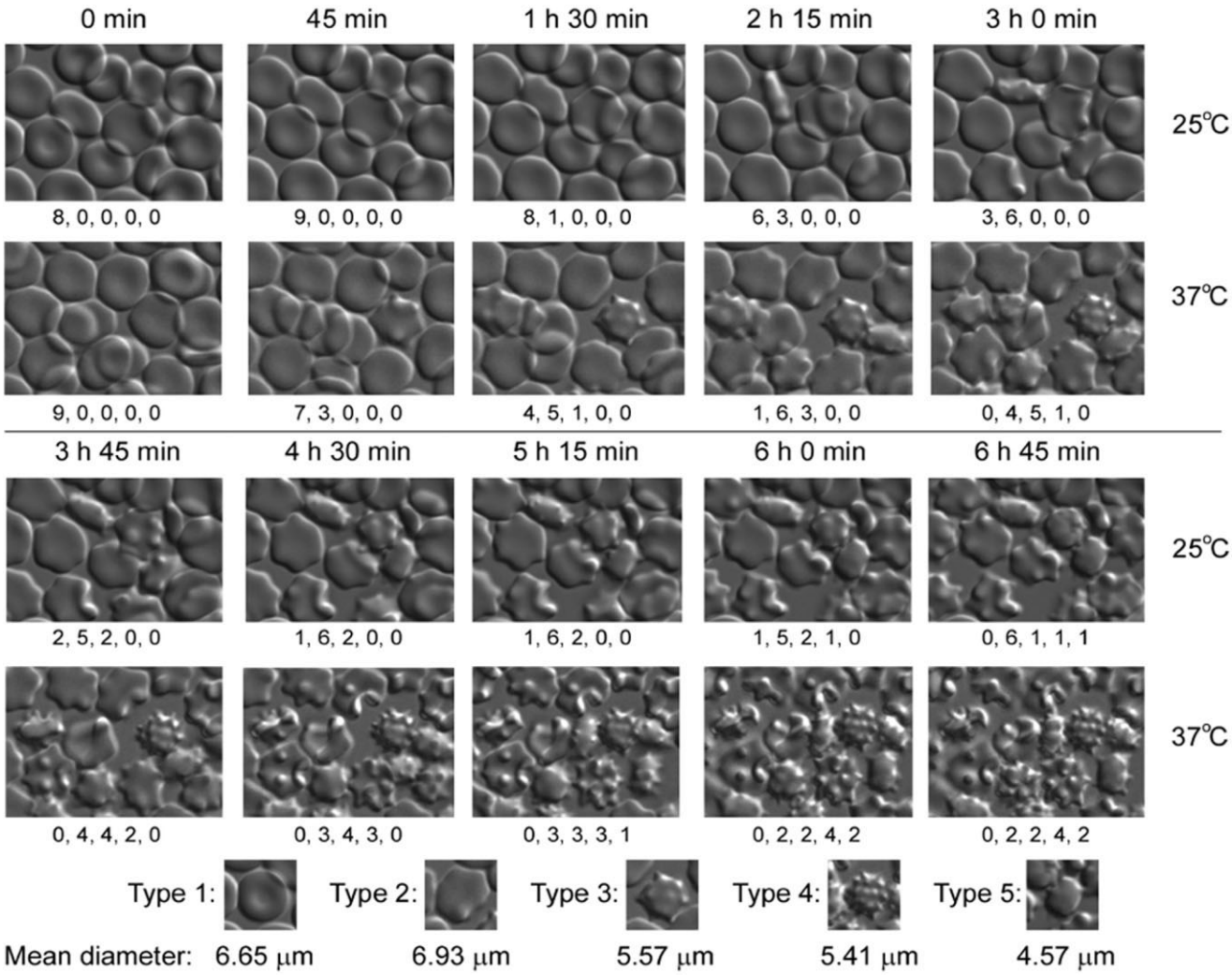

Figure 3. Microscope-recorded time course of RBC shape evolution after NaF (20 mM) addition at 25°C and 37°C. The numbers below each image indicate the number of each cell type in its corresponding panel in the form: number of Type 1, Type 2, Type 3, Type 4, and Type 5. The images at the bottom denote typical cell shapes for each Type. Initially, the shape of the RBCs was principally discocytes while at the end of the time course the RBCs were mostly spherocytes (Types 4 and 5).

experiments, the minima were at $q_{min1} = 1.9 \times 10^5\ m^{-1}$ and $q_{min2} = 3.7 \times 10^5\ m^{-1}$, whereas for the fast-measurement methods, these minima were at $q_{min1} = 2.0 \times 10^5\ m^{-1}$ and $q_{min2} = 4.2 \times 10^5\ m^{-1}$. These values are related in a simple way to the mean diameter of the cells (8,12) and correspond to an apparent diameter of 6.4 μm and 6.9 μm, and 6.1 μm and 5.8 μm, respectively, for classical and fast-measurement experiments. The water restriction effect occurs for low residual water signal, that is, around 0.2% and 0.02% for the first and second minimum, respectively. From these observations, we do not think the difference in the minimum q-values between the conventional and the fast-measurement PFGSTE pulse sequences could be attributed to any time-reduction issue. The inset in Figure 2 shows the characteristic distribution of mean-displacements (propagator) after applying: (1) a Blackman-Harris filter, (2) then a second derivative calculation, and (3) finally a Fourier transform. Discocyte RBCs had a maximum displacement value of 5.6 μm for both experiments; this corresponds to their inner diameter (27).

Fast NMR diffusion–diffraction experiments were run with the RBCs either all in the discocyte or the spherocyte shape, to investigate the ultimate capability of the pulse sequence to detect these extremes of shape; Figure 2b shows a characteristic q-space plot for both RBC shapes. Analysis of a q-space plot from spherocytes yielded one diffuse minimum and elevation of the curve at large values of q with a maximum at $\sim 2.0 \times 10^5\ m^{-1}$. The data were interpreted to indicate an apparent diameter of 5.0 μm. The characteristic mean-displacement distribution (inset in Fig. 2b) of spherocytes had a lower maximum displacement than discocytes at 2.8 μm. Although the discocyte diameter estimated from both the q-space experiment itself, and after postprocessing the data, were in very good agreement, there was expected to be a large variance in spherocyte shape as was born out by the light microscopy (see below). This important difference can be explained by the fact that a q-space plot is a weighted superposition of that from water inside, and that outside the RBCs, further complicated by rapid transmembrane exchange of water.

The new pulse sequence saved experiment time by a factor of eight. A *q*-space experiment required only 5 min for 64 points allowing the investigation of the kinetics of the system that evolved significantly on a timescale of ~10 min. Upon applying this method to RBC samples, it appeared that the estimate of the mean diameter was less after the signal processing, but the method had the merit of allowing a very clear distinction between both extremes of RBC shape. Therefore, the method was deemed to be satisfactory for studying shape evolution that was invoked by inhibiting glycolysis with NaF solution (21) (final concentration of NaF, 20 mM).

Light Microscopy and Fast-Recording NMR Diffusion–Diffraction

Shape evolution after the addition of NaF was monitored by both the fast-measurement pulse sequence and DIC light microscopy. The NMR *q*-space data were then processed to obtain displacement probabilities. The series of ~120 and ~65 NMR *q*-space plots recorded at 25°C and 37°C, respectively, and their associated displacement profiles were compiled as a movie stream (Supporting Video 1 and Supporting Video 2, respectively) that runs at ~5400 times the normal rate and thus facilitates the identification of all changes that occur (subpanels a and b indicate recordings at 25°C and 37°C, respectively). Figure 3 shows images and morphometric analyses of RBC shapes obtained by using DIC light microscopy. Time-lapse movies of images from these experiments are given in Supporting Video 3 (a and b were recorded at 25°C and 37°C, respectively). At any particular time the images clearly showed the presence of differently shaped RBCs from discocytes, and various forms of echinocytes and spherocytes. We used a classification scheme based on that of Bessis (4), scoring five different shapes: Type 1, smooth discocyte; Type 2, a form of early echinocyte that is a discocyte with "bumps" on an undulating membrane; Type 3, an echinocyte that is spheroidal with rounded membranous spikes; Type 4, echinocytes that are spherical with sharp membranous spikes; and Type 5, spheres with only very minor membranous protrusions, if any at all. Figure 3 shows, that whereas upon addition of NaF, after only 45 min, Type 2 cells were seen at 37°C. Approximately double this time was required to see significant numbers of Type 2 cells at 25°C. At 37°C, the time course of shape change was virtually complete after ~3.5 h, whereas it took ~5 h at 25°C.

Fast-recording NMR diffusion–diffraction experiments measure cell mean diameter from inside the cells. To compare both methods, we estimated this mean diameter in the microscope images, as well as scoring the cells among the five different types. The weighted mean diameter of the RBCs was found by summing the product of the number of cells of each type by the mean diameter of each type (see key in Fig. 3), and dividing this sum by the total number of cells. For the fast-recording diffusion–diffraction experiments we estimated the displacement probability values from data in the domain 1.4 to 7.0 μm, and rescaled the plots to give a maximum amplitude of 1.0 to the highest peak. Because the NMR processing systematically underestimates the diameter of spherocytes we rescaled the corresponding data. The mean diameter measured by the microscope was used as a reference for both discocytes and spherocytes and the NMR estimates were corrected to enable calculation of a revised NMR mean displacement scale. Thus, the mean diameter inside the RBCs in the NMR sample was estimated by applying the weighting formula noted above for the microscope images. Figure 4 shows the estimates of mean diameter over time for RBC suspensions at 25°C and 37°C.

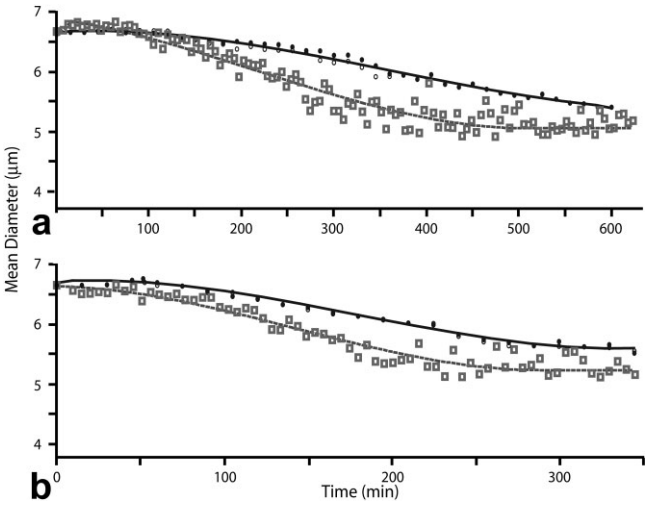

Figure 4. Evolution of the mean diameter of RBCs after poisoning with NaF (final concentration 20 mM) from microscope data (● and ○), scored a second time after severals days break, and from fast NMR diffusion–diffraction experiments (□). The data in (**a**) were recorded at 25°C, and for (**b**) at 37°C. The lines are to guide the eye. The mean diameters estimated from the microscope experiments were calculated by taking the sum of the number of cells of each type, multiplied by their inner mean diameter and then dividing the sum by the number of scored cells (thus giving a weighted mean). The fast NMR diffusion–diffraction experiments were processed from the distribution of mean displacements in the domain 1.4 to 7.0 μm (equivalent to peak areas). Because the mean displacement was underestimated, these values were rescaled prior to comparison with the microscope data; the scaling factor was applied to NMR data to specify the same mean diameter at the beginning of both types of experiment. This minor scaling was the same for both temperatures and was 1.07.

In the fast-recording NMR *q*-space experiments, estimates of mean diameters decreased faster than for the parallel microscope experiments. Estimates of mean diameters were in good agreement at the beginning and at the end of the experiment for both temperatures. The difference at the end of the experiment was of the order of 0.25 μm, that is, less than 5% of the mean value. The difference in the middle of the time course was the greatest with a disparity of ~10% of the calculated mean diameter (~0.6 μm). The scaling factors applied to the diameters estimated from the NMR datasets were very close to 1 (1.07 for both temperatures).

We estimated the fraction (%) of discocytes at each time by *q*-space analysis. Cell mean diameter increased slightly from discocyte to echinocyte type 2 (6.6 to 6.9 μm, respectively) and then decreased along all different

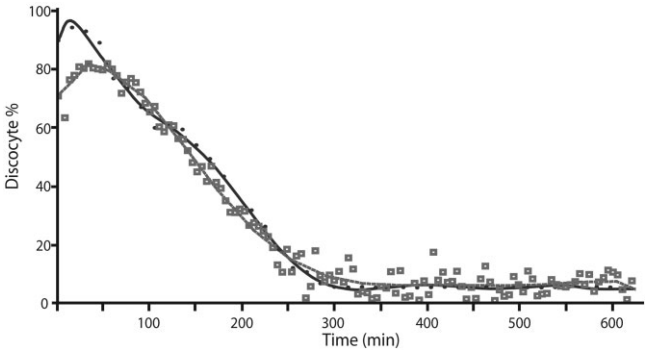

Figure 5. Evolution of the discocyte percentage as measured by fast measurement of diffusion NMR (□) and by the microscope (●) at 25°C.

echinocyte types to reach the lowest value for spherocytes (4.6 μm). Discocyte percentage was estimated from the ^1H_2O diffusion–displacement probability of these cells, related to the sum of all displacement probabilities from spherocyte to discocyte mean diameters. Figure 5 compares the percentage of discocytes for *q*-space and microscope experiments. A difference was observed for data acquired at the beginning of the experiment and then curve overlap for both techniques was good.

^{31}P NMR and Fast-Recording NMR Diffusion–Diffraction

Stacked plots of ^{31}P NMR spectra recorded at the indicated times and obtained for both 25°C and 37°C are shown in Figure 6a–b. To obtain the ATP concentration, the integral of the ATP-γP peak, and an internal chemical shift and peak-intensity reference (TEP) were used. Time courses correlating ATP concentration and discocyte fraction (calculated as noted above) are given in the insets of Figure 6a–b. Figure 6c shows the correlation between the mean internal diameter of the RBCs in the sample and the ATP concentration.

The insets of Figure 6a–b show that the ATP concentration decreased immediately after adding NaF to the sample, whereas the fraction of the RBC population that was discocytes was initially unchanged and constant. The almost immediate decline of the ATP peaks is explained by the fluoride ion rapidly entering the cells and inhibiting enolase thus preventing ATP regeneration (12). Cell shape evolution was delayed to ~80 min at 25°C and ~40 min at 37°C, and it occurred when the ATP concentration inside the cells was low (~0.5 mM). When the ATP concentration was 0.0 mM, ~40% of the cells were still discocytes, and this percentage declined further over time. Figure 6c exhibits these effects showing a constant mean diameter until a low intracellular ATP concentration (~0.2 mM), and then a decrease of cell mean diameter for lower ATP concentrations.

DISCUSSION

We demonstrated that the rapidly recorded NMR *q*-space experiment is capable of probing the evolution of RBC shapes from discocytes to spherocytes, with a recycle time (temporal resolution) of only a few minutes. Exploiting data from *q*-space plots gave estimates of mean diameters of RBCs that were in good agreement with those measured running a classical diffusion pulse sequence. Using Blackman-Harris second-derivative data processing, spherocyte mean diameters were slightly underestimated; but the method has the advantage of being easily automated (we wrote our program in *Mathematica*). An explanation for this effect may be that the actual diameter available to diffusing water inside the RBC is less than expected because of the thickness of the cytoskeleton and possible organization of hemoglobin on it, and/or if there was misalignment of the cells with the static magnetic field (28). Indeed, to obtain the characteristic *q*-space plot from a sample of discocytes the cells must be almost completely aligned in the direction of the static magnetic field of the spectrometer, $\mathbf{B}_0$ (8). This situation pertains at the beginning of the experiments but for other cell shapes (especially Types 3 and 4), the cells have no axis of symmetry and are not systematically aligned with $\mathbf{B}_0$, thus decreasing the apparent mean diameter of the RBC population. Due to their symmetry, spherical cells are not affected by this phenomenon.

The ^{31}P NMR spectra enabled ready noninvasive estimation of ATP concentrations in RBCs. Furthermore, because the ATP-γP and ADP-βP resonances were well resolved the concentration estimate could be reliably based on this peak alone, it has greater signal to noise than the ATP-βP peak that is usually used with other tissues. The ATP-βP peak usually is chosen because it has the advantage that it is exclusively due to ATP, but it suffers from much poorer signal to noise because of homonuclear scalar-coupling making it a triplet, whereas the ATP-γP peak is a more prominent doublet. Previous studies using standard biochemical and hematological laboratory methods established the likely dependence of RBC shape on cytoplasmic ATP concentration (2,3). The present results are in accordance with this earlier work (2,3), although there was a long lag before the shape changes occurred. The ATP concentration was temperature dependent as were the shape changes; but as just noted, the transition from discocyte to echinocyte appeared to correlate with ATP concentration only when it was less than half the normal value.

A comparison of the data obtained from the microscope and *q*-space plots (Fig. 4) reveals a difference between the estimates of cell diameter that is largest when the cells are a complex mixture of different forms of echinocytes. For almost pure discocytes at zero time, and spheres after many hours, the comparison is better. We ascribe this effect to an incomplete understanding of the distortion of the cytoskeleton in echinocytes and how this restricts the diffusion of water inside them, and in also how this shape variation renders an estimate of the diameter less certain than with the "smoother" forms of the cells. Another factor is likely to be the difference in experimental conditions used with the methods, especially the dilute hematocrit and less stringent thermal control in microscopy.

In conclusion, RBC shape evolution can readily be measured by an NMR method with a time-resolution of

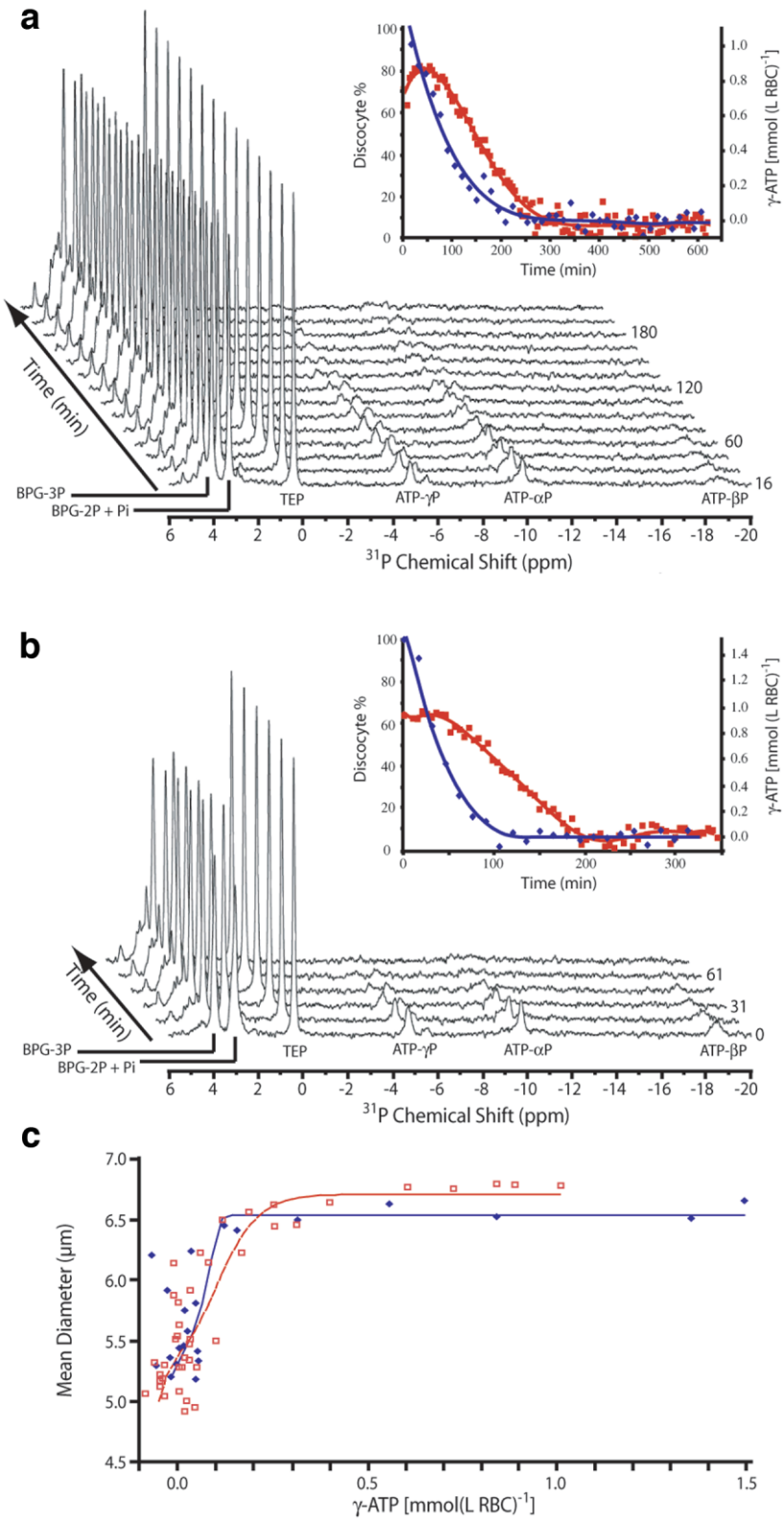

Figure 6. ^{31}P NMR stacked plots obtained after inhibiting glycolysis in a sample of RBCs with NaF (final concentration 20 mM). The time course graph illustrates both ATP-γP concentration decreasing (◆) from ^{31}P NMR and the discocyte RBC percentage (■) evolution from fast NMR diffusion–diffraction experiments. The fraction of the cells that were discocytes was calculated by assuming that all RBCs had a mean diameter, after data processing, that corresponded either to a discocyte or a spherocyte. (**a**) Experiments were recorded at 25°C; and, (**b**) were recorded at 37°C. The evolution of cell mean diameter as measured by NMR is correlated with the intracellular ATP concentration in (**c**) at 25°C (□) and 37°C (◆). The lines in the insets are to guide the eye.

minutes and processed to obtain an estimate of the mean diameter by an automatic program that is an elegant adjunct/alternative to the laborious scoring processes used for microscope data. Microscope experiments often use dilute cell suspensions for which temperature control on the mechanical stage is difficult, and concurrent or subsequent biochemical analysis of the small samples is precluded. The new approach can be used to investigate RBC shape modifications that occur with various xenobiotic compounds, and to achieve better understanding of the active mechanisms at work in maintaining RBC shape in various diseases (e.g., sickle cell anaemia, malaria, and hereditary sphero- and elliptocytosis). Other applications, based

on analyzing restricted diffusion of probe molecules in parallel with other biochemical and biophysical measurements made with NMR, exist in the biological and chemical arenas.

ACKNOWLEDGMENTS

We thank Dr. Bill Bubb for his NMR expertise and Dr. Stéphane Viel and Professor Bernard Ancian for their helpful discussions.

REFERENCES

1. Bortner CD, Sifre MI, Cidlowski JA. New approaches for determining apoptotic volume decrease in cells. In: Haussinger D, Sies H, editors. Methods enzymol, vol. 428. San Diego, CA: Academic Press; 2007. p 161–181.
2. Féo CJ, Leblond PF. The discocyte–echinocyte transformation: comparison of normal and ATP-enriched human erythrocytes. Blood 1974;44:639–647.
3. Backman L. Shape control in the human red cell. J Cell Sci 1986; 80:281–298.
4. Bessis M. Red cell shapes: an illustrated classification and its rationales. Nouv Rev Fr Hematol 1972;12:721–746.
5. Branton D, Elgsaeter A, Stokke BT, Mikkelsen A. The molecular basis of erythrocyte shape. Science 1986;234:1217–1223.
6. Elgsaeter A, Mikkelsen A. Shapes and shape changes in vitro in normal red blood cells. Biochim Biophys Acta Biomembr 1991; 1071:273–290.
7. Grimes A. Human red cell metabolism. Oxford: Wiley-Blackwell; 1980. p 126.
8. Kuchel PW, Coy A, Stilbs P. NMR "diffusion–diffraction" of water revealing alignment of erythrocytes in a magnetic field and their dimensions and membrane transport characteristics. Magn Reson Med 1997;37:637–643.
9. Callaghan PT, Coy A, MacGowan D, Packer KJ, Zelaya FO. Diffraction-like effects in NMR diffusion studies of fluids in porous solids. Nature 1991;351:467–469.
10. Callaghan PT. Pulsed-gradient spin-echo NMR for planar, cylindrical, and spherical pores under conditions of wall relaxation. J Magn Reson A 1995;113:53–59.
11. Söderman O, Jonsson B. Restricted diffusion in cylindrical geometry. J Magn Reson A 1995;117:94–97.
12. Torres AM, Michniewicz RJ, Chapman BE, Young GAR, Kuchel PW. Characterisation of erythrocyte shapes and sizes by NMR diffusion–diffraction of water: correlations with electron micrographs. Magn Reson Imag 1998;16:423–434.
13. King MD, Houseman J, Roussel SA, Van Bruggen N, Williams SR, Gadian DG. *q*-Space imaging of the brain. Magn Reson Med 1994; 32:707–713.
14. King MD, Houseman J, Gadian DG, Connelly A. Localized *q*-space imaging of the mouse brain. Magn Reson Med 1997;38:930–937.
15. Assaf Y, Cohen Y. Structural information in neuronal tissue as revealed by *q*-space diffusion NMR spectroscopy of metabolites in bovine optic nerve. NMR Biomed 1999;12:335–344.
16. Bar-Shir A, Cohen Y. High *b*-value *q*-space diffusion MRS of nerves: structural information and comparison with histological evidence. NMR Biomed 2008;21:165–174.
17. Basser PJ, Mattiello J, LeBihan D. MR diffusion tensor spectroscopy and imaging. Biophys J 1994;66:259–267.
18. Schaefer PW, Grant PE, Gonzalez RG. Diffusion-weighted MR imaging of the brain. Radiology 2000;217:331–345.
19. Le Bihan D. Looking into the functional architecture of the brain with diffusion MRI. Nat Rev Neurosci 2003;4:469–480.
20. Kärger J, Heink W. The propagator representation of molecular transport in microporous crystallites. J Magn Reson 1983;51: 1–7.
21. Kuchel PW, Eykyn TR, Regan DG. Measurement of compartment size in *q*-space experiments: Fourier transform of the second derivative. Magn Reson Med 2004;52:907–912.
22. Pages G, Kuchel PW. NMR methods for the fast-recording of diffusion. In: Brandani S, Chmelik C, Kärger J, Volpe R, editors. Diffusion fundamentals II. Leipzig: Leipziger Universitätsverlag; 2007. p 52–68.
23. Pelta MD, Morris GA, Stchedroff MJ, Hammond SJ. A one-shot sequence for high-resolution diffusion-ordered spectroscopy. Magn Reson Chem 2002;40:S147–S152.
24. Wu DH, Chen AD, Johnson CS. An improved diffusion-ordered spectroscopy experiment incorporating bipolar-gradient pulses. J Magn Reson A 1995;115:260–264.
25. Kirk K, Raftos JE, Kuchel PW. Triethyl phosphate as an internal ^{31}P NMR reference in biological samples. J Magn Reson 1986;70:484–487.
26. Shaka AJ, Keeler J, Freeman R. Evaluation of a new broadband decoupling sequence: WALTZ-16. J Magn Reson 1983;53:313–340.
27. Kuchel PW, Pages G. NMR diffusion diffraction and diffusion interference from cells. In: Brandani S, Chmelik C, Kärger J, Volpe R, editors. Diffusion fundamentals II. Leipzig: Leipziger Universitätsverlag; 2007. p 345–360.
28. Avram L, Assaf Y, Cohen Y. The effect of rotational angle and experimental parameters on the diffraction patterns and microstructural information obtained from *q*-space diffusion NMR: implication for diffusion in white matter fibers. J Magn Reson 2004; 169:30–38.